Nano Research
2022, 15(2): 1145–1152

ISSN 1998-0124 CN 11-5974/O4
https://doi.org/10.1007/s12274-021-3617-3

Research Article

Metallocorrole-based porous organic polymers as a heterogeneous catalytic nanoplatform for efficient carbon dioxide conversion

Yanming Zhao[1,2], Yunlei Peng[3], Chuan Shan[4], Zhou Lu[2], Lukasz Wojtas[4], Zhenjie Zhang[3], Bao Zhang[1] (✉), Yaqing Feng[1,5], and Shengqian Ma[2] (✉)

[1] *School of Chemical Engineering and Technology, Tianjin University, Tianjin 300350, China*
[2] *Department of Chemistry, University of North Texas, Denton, Texas 76201, USA*
[3] *College of Chemistry, Nankai University, Tianjin 300071, China*
[4] *Department of Chemistry, University of South Florida, Tampa, Florida 33620, USA*
[5] *Collaborative Innovation Center of Chemical Science and Engineering, Tianjin 300072, China*

Received: 15 April 2021 / **Revised:** 20 May 2021 / **Accepted:** 22 May 2021

ABSTRACT

Metallocorrole macrocycles that represent a burgeoning class of attractive metal-complexes from the porphyrinoid family, have attracted great interest in recent years owing to their unique structure and excellent performance revealed in many fields, yet further functionalization through incorporating these motifs into porous nanomaterials employing the bottom-up approach is still scarce and remains synthetically challenging. Here, we report the targeted synthesis of porous organic polymers (POPs) constructed from custom-designed Mn and Fe–corrole complex building units, respectively denoted as **CorPOP-1(Mn)** and **CorPOP-1(FeCl)**. Specifically, the robust **CorPOP-1(Mn)** bearing Mn-corrole active centers displays superior heterogeneous catalytic activity toward solvent-free cycloaddition of carbon dioxide (CO_2) with epoxides to form cyclic carbonates under mild reaction conditions as compared with the homogeneous counterpart. **CorPOP-1(Mn)** can be easily recycled and does not show significant loss of reactivity after seven successive cycles. This work highlights the potential of metallocorrole-based porous solid catalysts for targeting CO_2 transformations, and would provide a guide for the task-specific development of more corrole-based multifunctional materials for extended applications.

KEYWORDS

corrole, porphyrinoid derivatives, heterogenization, porous organic polymers (POPs), CO_2 conversion, heterogeneous catalysis

1 Introduction

Porphyrinoid derivatives which represent the most important class of pyrrole-based macrocycles have long been a topic of research [1–5]. Among these tetrapyrrolic compounds, corroles as the fully aromatic analogues of the corrin ligands found in B_{12} cofactors, have received increasing attention not only due to the progress in the facile synthetic method [6] but also their unique structural characteristics of the direct pyrrole-pyrrole linkage, three protons in the inner core and contracted ring, affording attractive physicochemical properties [7–9]. Recent advances in the research field of corroles have made them a burgeoning class of molecules holding considerable promise in diverse fields including catalysis, energy conversion, and biology [10–13]. Nonetheless, from the viewpoint of functional versatility, the field of corroles is still in its early stage especially when compared with the extensive investigation of porphyrins in both science and technology areas. Therefore, there is a lot of room for targeting further functionalization of corroles and their corresponding metalated complexes toward the materials development and expanded applications.

Especially, the unique inner core with three protons in the corrole structures [14, 15] enables distinctive coordination environment for the incorporation of metals with unusual oxidation states leading to rich metallocorrole catalogues, some of which have been reported with the encouraging electrocatalytic [16] and organocatalytic [17–22] activities. However, a series of shortcomings have been recognized for molecular metallocorroles based homogeneous catalysis systems: the deactivation of catalyst due to self-oxidation resulting in the reduced catalytic activity, poor recyclability of catalyst and thus the decreased lifetime, and tedious separation and purification procedure for the final product leading to cost increase. The emergence of porous materials-based heterogeneous catalysis [23–26] systems offers some possibilities to compensate the above shortcomings, wherein the direct incorporation of catalytically active moieties into the pore walls of porous solid supports represents one of the most intriguing strategies to bridge homogeneous and heterogeneous catalysis [27, 28]. This bottom-up approach facilitates the modulation of framework materials with tailor-made porous structure and surface chemistry, and provides an opportunity for the design of polymeric networks with various functionalities for use as catalysts.

Bearing the heterogenization of molecular catalysts in mind, much effort has been devoted to exploiting advanced porous materials as designable platforms for realizing the excellent catalytic performance as compared to their molecular

Address correspondence to Bao Zhang, baozhang@tju.edu.cn; Shengqian Ma, Shengqian.Ma@unt.edu

counterparts. In the past two decades, the field of porous materials has undergone rapid growth, with a number of new porous materials well developed for heterogeneous catalysis, such as metal–organic frameworks (MOFs) [24], covalent organic frameworks (COFs) [25], and porous organic polymers (POPs) [26]. POPs constructed from purely organic monomers via strong covalent bonds [29–31], are promising intermediary candidates because of their high surface areas, tunable pore sizes, extraordinary stability, and chemically adjustable compositions, a combination that most existing materials even some MOFs and COFs lack of, whereas these two crystalline framework materials assembled through reversible bonds are generally susceptible to decomposition upon exposure to harsh conditions, resulting in an inevitable structural decomposition. Pioneering work done using a corrole-based MOF material (Corrole-MOF-1(Fe)) focused on the metallocorrole-induced heterogeneous catalysis for effectively catalyzing Diels-Alder reactions [32]; however, the framework stability issue is a concern, given that the supercritical CO_2 drying is an indispensable procedure to ensure the structural integrity of this framework during material activation processes, thus to a certain extent hampering its use in a wide range of applications. Hence, considering the shortcomings of metallocorroles in homogeneous catalysis and the aforementioned structural merits of POP framework materials, it is highly desirable to construct metallcorrole-based POP heterogeneous catalysts, which would also provide a high density of accessible isolated active species avoiding agglomeration in catalytic reactions.

In this study, we report the bottom-up synthesis of novel corrole-based POPs by reacting the custom-designed metallocorrole complexes MPFBC, M = Mn, FeCl and PFBC = 10-(pentafluorophenyl)-5,15-bis(*p*-bromophenyl)corrole, with the triarylamine derivative TTDPA via the classic Suzuki-Miyaura coupling (shown in Scheme 1) for application in heterogeneous catalysis, which has rarely been explored [32, 33]. These new corrole-based POPs, hereafter denoted as **CorPOP-1(Mn)** and **CorPOP-1(FeCl)**, exhibit large Brunauer-Emmett-Teller (BET) surface areas, good CO_2 adsorption capacity, and prominent stability. Interestingly, **CorPOP-1(Mn)** shows the excellent catalytic performance for the cycloaddition of CO_2 and epoxides to yield cyclic carbonates under mild reaction conditions, greatly outperforming the homogeneous counterpart, with excellent recyclability. The present results open new avenues for the construction of multifunctional corrole-based porous solid materials in widely applicable fields.

2 Experimental section

All chemicals and solvents, unless otherwise mentioned, are commercially available and used without further purification. 2,2'-[(4-Bromophenyl)methylene]bis[1*H*-pyrrole] and Tri[4-(4,4,5,5-tetramethyl-1,3,2-dioxaborolan-2-yl)phenyl]amine (TTDPA) used for the synthesis of corrole-based POPs were prepared based on the previous literatures [34, 35].

2.1 Synthesis of free-base H_3PFBC

2,2'-[(4-Bromophenyl)methylene]bis[1*H*-pyrrole] (4 mmol, 1,204 mg) and pentafluorobenzaldehyde (2 mmol, 396 mg) were dissolved in 200 mL CH_3OH, and then 200 mL H_2O was added. Subsequently, 10 mL concentrated HCl was added, and the reaction was stirred at room temperature for 3 h. After that, the mixture was extracted with $CHCl_3$, and the organic layer was washed twice with H_2O, dried ($MgSO_4$), filtered, and diluted to 800 mL with $CHCl_3$. And then, chloranil (6 mmol, 1,476 mg) was added, and the mixture was stirred overnight at room temperature. The reaction mixture was evaporated to dryness, and the crude product was purified by chromatography with CH_2Cl_2/hexane (1/2, by vol.), finally with dark-red product 10-(pentafluorophenyl)-5,15-bis(p-bromophenyl)corrole (H_3PFBC) obtained (650 mg, 42% yield) [6]. UV–Vis (CH_2Cl_2) λ_{max}: 415, 577, 605, 643 nm (Fig. S3 in the Electronic Supplementary Material (ESM)). ^{1}H NMR (400 MHz, DMSO) δ: 9.04 (s, 2H),

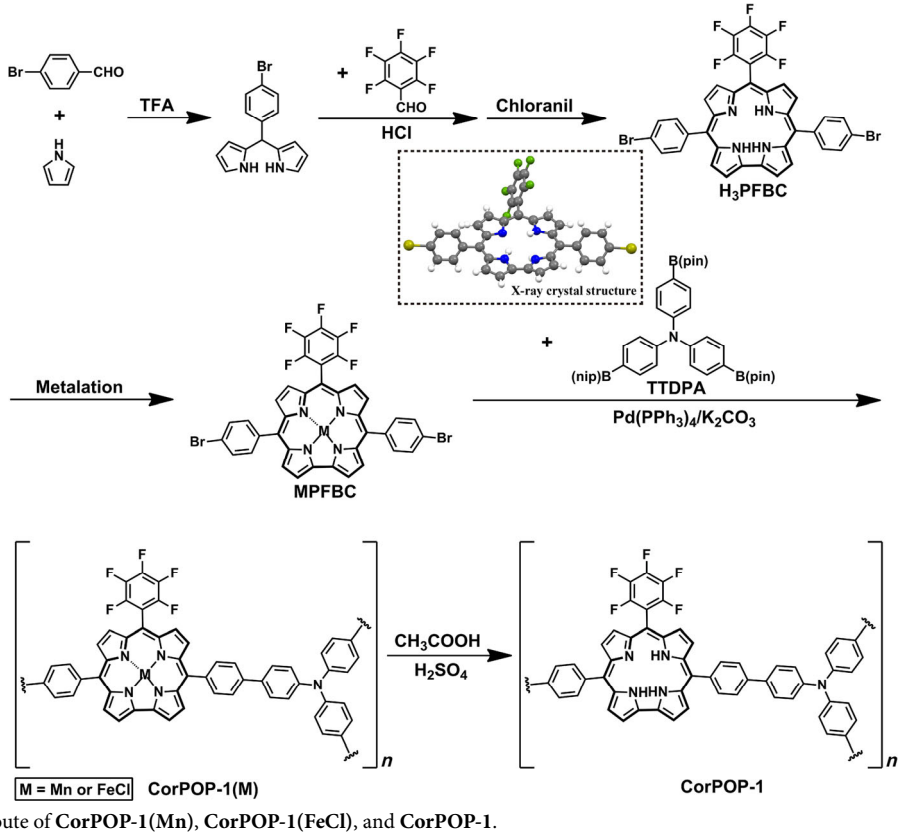

Scheme 1 Synthetic route of **CorPOP-1(Mn)**, **CorPOP-1(FeCl)**, and **CorPOP-1**.

8.85 (s, 2H), 8.67 (s, 2H), 8.42 (s, 2H), 8.24 (s, 4H), 8.049–8.066 (d, J = 6.8 Hz, 4H); MALDI-TOF-MS: m/z Calcd. for $C_{37}H_{19}Br_2N_4F_5$, 773.99; Found, 774.36 $[M+H]^+$.

2.2 Synthesis of metalated MnPFBC

A solution of H_3PFBC (0.26 mmol, 200 mg) and excess of manganese(II) acetate tetrahydrate (5.2 mmol, 1,274 mg) in 200 mL of CH_2Cl_2/CH_3OH (50/50, by vol.) was heated to reflux for 3 h in the dark. After evaporating the solvent, the crude product was purified by chromatography (basic aluminum oxide), using CH_2Cl_2/hexane (1/1, by vol.) as eluents, finally obtained with dark-green product [10-(pentafluorophenyl)-5,15-bis(*p*-bromophenyl)corrolato]-Mn (MnPFBC) (186 mg, 87% yield) [36]. UV–Vis (CH_2Cl_2) λ_{max}: 404, 423, 587, 631 nm (Fig. S3 in the ESM). MALDI-TOF-MS: m/z Calcd. for $C_{37}H_{16}Br_2N_4F_5Mn$, 825.90; Found, 826.15 $[M+H]^+$.

2.3 Synthesis of metalated FeClPFBC

A solution of H_3PFBC (0.26 mmol, 200 mg) and excess of ferrous chloride tetrahydrate (5.2 mmol, 1,034 mg) in 25 mL of DMF was heated to reflux under N_2 for 2 h in the dark. After cooling to room temperature, 45 mL HCl aqueous solution (3 mol/L) was dropwise added to the mixture. The resulted precipitate was filtrated and dissolved in CH_2Cl_2 (60 mL), and washed with 7% aqueous HCl (45 mL × 3). The organic layer was dried over $MgSO_4$, filtered, and concentrated under reduced pressure to give [10-(pentafluorophenyl)-5,15-bis(*p*-bromophenyl)corrolato]-Fe (FeClPFBC) as the red-brown solid product (183 mg, 82% yield) [32]. UV–Vis (CH_2Cl_2) λ_{max}: 366, 409, 625 nm (Fig. S3 in the ESM). MALDI-TOF-MS: m/z Calcd. for $C_{37}H_{16}Br_2N_4F_5FeCl$, 861.87; Found, 862.21 $[M+H]^+$.

2.4 Preparation of CorPOP-1(Mn) and CorPOP-1(FeCl)

Under N_2 atmosphere, MnPFBC (0.12 mmol, 100 mg), TTDPA (0.16 mmol, 100 mg), potassium carbonate (1.45 mmol, 200 mg), tetrakis(triphenylphosphine)palladium(0) (0.024 mmol, 28 mg), 1,4-dioxane (20 mL), and deionized water (5 mL) was added to a dried 50 mL Schlenk tube. The mixture was magnetically stirred at 110 °C for 72 h, and cooled down to room temperature. Subsequently, the mixture was poured into water and the precipitate was collected by filtration, and then washed with H_2O, THF, CH_3OH, and acetone to remove the unreacted monomer and residual catalyst. After rigorously washed by Soxhlet extractions for 24 h with THF, CH_3OH, and acetone respectively, and then dried in vacuum at 80 °C for 12 h, **CorPOP-1(Mn)** (92 mg) was obtained as dark powder in 93% isolated yield. For preparation of **CorPOP-1(FeCl)**, FeClPFBC (0.12 mmol, 116 mg) instead of MnPFBC was used in the reaction following the same procedure.

2.5 Preparation of CorPOP-1

In order to eliminate the effect of metalation of corrole molecules in coupling reaction, we obtained metal-free corrole-based POP (**CorPOP-1**) through post-synthesis, i.e., demetalation reaction of **CorPOP-1(Mn)** [37]. 20 mL CH_3COOH/H_2SO_4 (3/1, by vol.) and 100 mg **CorPOP-1(Mn)** were added into a 50 mL round-bottom flask and stirred at 90 °C for 12 h. The solid product was collected and rigorously washed with H_2O, THF, CH_3OH, and acetone. After being suction dried for 2 h and dried under vacuum at 80 °C for 12 h, **CorPOP-1** (85 mg) was obtained as dark powder in 91% isolated yield.

2.6 Catalytic cycloaddition of CO_2 to epoxides

A typical procedure for a solvent-free cycloaddition reaction with atmospheric CO_2 was conducted in a 25 mL Schlenk tube. For a typical run, the epoxide (13 mmol), catalyst (0.013 mmol based on active sites, 0.1 mol%) (Fig. S13 in the ESM), and cocatalyst tetrabutylammonium bromide (TBAB, 0.52 mmol, 4 mol.%) were added into the tube that was vacuum-sealed and purged with CO_2 by adding a balloon. And then, the tube was placed in a preheated oil bath with a designated temperature while allowed to stir for a designated time frame. The product yield was determined by comparison of the ^{1}H NMR integrals of the corresponding protons in the starting material (epoxide) and the product (cyclic carbonate). The catalyst was recovered by filtration and subsequently washed rigorously with dichloromethane. After dried under vacuum at 80 °C for 2 h, the obtained solid POP catalyst was used for the next cycle. Further characterizations were carried out to investigate the recyclability and stability of the CorPOP catalysts.

3 Results and discussion

3.1 Design and synthesis of CorPOPs

We designed the monomer MPFBC by attaching the pentafluorophenyl moiety to the meso-10 position on the corrole skeleton as the bidentate building block, different from the tridentate precursors in the fabrication of corrole-based porous crystalline materials previously reported [32, 38], which is based on the following considerations: on one hand, the electron-withdrawing nature of pentafluorophenyl group can improve the stability of metallocorrole complexes; on the other hand, it can reduce the electron density of coordination metals in the corrole ring and increase their Lewis acidity, thus contributing to the boosted catalytic reactivity. Meanwhile, the other component introduced for the construction of CorPOPs is a triarylamine derivative TTDPA, which possesses the distorted, nonplanar structure imparting the POPs with favorable porosities. We reasoned that such an integration would allow for the observation of their potential in tailoring to heterogeneous catalysis.

The synthesis of the MPFBC monomer relied on the formation of the free-base corrole H_3PFBC through two independent steps [6], including the acid-mediated electrophilic substitution reaction and the oxidative ring closure reaction, followed by metalation to generate metallocorrole complexes [10-(pentafluorophenyl)-5,15-bis(*p*-bromophenyl)corrolato]-M (M = Mn and FeCl). The resultant precursors were treated with TTDPA in the presence of a Pd(0) catalyst in 1,4-dioxane/H_2O at 110 °C to afford **CorPOP-1(M)** (Scheme 1). To meet the requirements for a comparative study and the better understanding of metallocorrole-based POPs, we also successfully prepared the metal-free **CorPOP-1** by a second acid-induced demetalation reaction.

3.2 Structural characterization

The crystallinity and regularity of CorPOPs reported here were investigated by powder X-ray diffraction (PXRD) analysis (Fig. S5 in the ESM). The PXRD patterns reveal that CorPOPs are amorphous rather than crystalline, which is manifested by the existing wide peaks in the 2θ range of 10°–30°. The Fourier transform infrared (FTIR) and inductively coupled plasma optical emission spectrometry (ICP-OES) studies were employed to determine the structural characteristics of CorPOPs as compared to those of their corresponding counterparts. The disappearance of the C–Br characteristic band at 460 and 490 cm^{-1} respectively for **CorPOP-(Mn)** and **CorPOP-1(FeCl)** proves the successful polymerization of metallocorrole incorporated POPs (Fig. S6 in the ESM). For **CorPOP-1**, the absence of the peak located at 966 cm^{-1}, which is assigned to the Mn–N typical vibration band in the corrole ring, by comparison with

CorPOP-1(Mn), suggests the demetalation procedure with the desired metal-free CorPOP material. Meanwhile, it can be observed with the characteristic stretching vibration band at 932 cm^{-1} in the tested FTIR spectrum of **CorPOP-1(FeCl)**, which is ascribed to the coordinated Fe–N bond of the FeClPFBC complex. ICP-OES analysis confirms a Mn loading of 6.1 wt.% for **CorPOP-1(Mn)**, whereas **CorPOP-1** shows a Mn loading of < 0.1 wt.%, further suggesting that almost all the coordinated Mn can be removed upon the subsequent rigorous acid treatment to afford the free-base CorPOP. These three obtained polymers are chemically stable and completely insoluble in water and common organic solvents; they also exhibit high thermal stability up to 400 °C under N_2 atmosphere as assessed by the thermogravimetric analysis (TGA) (Fig. S7 in the ESM), indicative of their structural robustness. The **CorPOP-1(Mn)**, modelled computationally as a representative, has a three-dimensional porous framework structure originating from the three-pronged component TTDPA (Fig. 1(a)), which is favorable for heterogeneous catalysis applications.

Solid-state ^{13}C cross-polarization magic-angle spinning (CP/MAS) NMR studies were performed to further analyze the chemical structures of CorPOPs. Unfortunately, the ^{13}C CP/MAS NMR spectra could not be obtained for **CorPOP-1(Mn)** and **CorPOP-1(FeCl)** due to their paramagnetic nature (Fig. S8 in the ESM). However, the ^{13}C CP/MAS NMR spectrum of metal-free **CorPOP-1** was obtained (Fig. 1(b)). By comparison with H_3PFBC (Fig. S9 in the ESM), **CorPOP-1** displays only two broad peaks along with some shoulder peaks between 110 and 150 ppm ascribing to the overlap of the aromatic carbon and corrole ring carbon resonance. The peak at 119.8 ppm is attributed to the meso carbon atoms of the corrole ring. The peak located at 144.9 ppm is assigned to the carbon atoms bonding to nitrogen atoms on the corrole skeleton and triarylamine skeleton. The two broad peaks at 126.1 and 140.2 ppm are ascribed to the remaining carbon atoms of the pyrrole rings and aromatic rings. In order to disclose the morphologies and composition distributions of CorPOPs, scanning electron microscopy (SEM), transmission electron microscope (TEM) and energy dispersive X-ray (EDX) techniques were utilized. SEM images (Fig. 2(a) and Figs. S10 and S11 in the ESM) manifest that CorPOPs consist of smooth-faced, spherical-shaped nanoparticles with a narrow size distribution in the range of 200–600 nm, further demonstrated by the TEM images (Fig. 2(b)). The EDX spectrum confirms the existence of C, N, F, and Mn elements in the prepared **CorPOP-1(Mn)** (Fig. 2(h)), and the elemental mapping images further indicate their homogeneous distributions over the entire polymeric architecture (Figs. 2(c)–2(g)).

The permanent porosities of CorPOPs were evaluated by

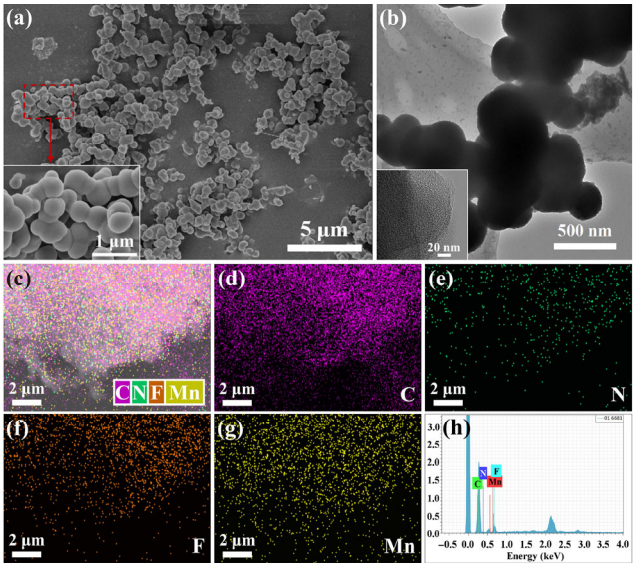

Figure 2 Morphological and compositional characterizations of **CorPOP-1(Mn)**. (a) SEM (inset) images. (b) TEM (inset) images. (c)–(g) Elemental mapping images. (h) EDX spectrum.

N_2 sorption measurements at 77 K (Fig. 3(a)). Employing the BET model, the specific surface areas were calculated to be 492, 416, and 351 $m^2 \cdot g^{-1}$ for **CorPOP-1(Mn)**, **CorPOP-1**, and **CorPOP-1(FeCl)**, respectively. These three corrole-based polymers shown here all show a type I sorption isotherm with profound hysteresis that can be attributed to the existence of small micropores and a kinetic barrier of adsorption [39]. Based on the nonlocal density functional theory (NLDFT) method, the pore size distributions were obtained with the dominant pore width centered at 1.6 nm and a broad hump in the mesoporous region ranging from about 2.0 to 5.0 nm. Specifically, this hierarchically porous structure is favorable for the mass transport in the catalytic reactions. CO_2 sorption properties of these polymeric materials were also studied employing the volumetric method at 298 K (Fig. 3(b)), in which the isotherms display the reversible adsorption capacity. Interestingly, it is found that the CO_2 uptake capacities reach moderate values of 47, 45, and 40 $mg \cdot g^{-1}$ for **CorPOP-1(Mn)**, **CorPOP-1**, and **CorPOP-1(FeCl)**, respectively at 1 bar and 298 K. In addition, the shapes of the gas (N_2/CO_2) sorption isotherms for **CorPOP-1(Mn)** and **CorPOP-1** are almost identical, indicating that the demetalation procedure in the preparation of **CorPOP-1** did not change the porosity significantly. Accordingly, the above results suggest that CorPOPs have the potential to combine the abilities to capture and convert CO_2, a combination that homogeneous catalysts lack.

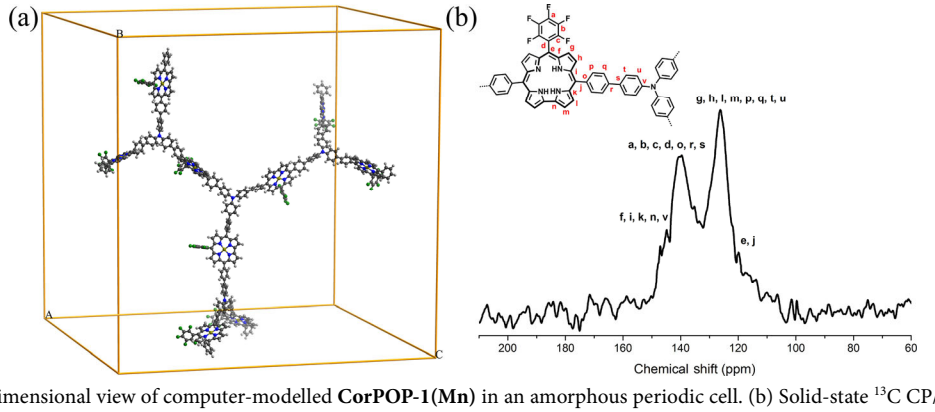

Figure 1 (a) Three-dimensional view of computer-modelled **CorPOP-1(Mn)** in an amorphous periodic cell. (b) Solid-state ^{13}C CP/MAS NMR spectrum of **CorPOP-1**.

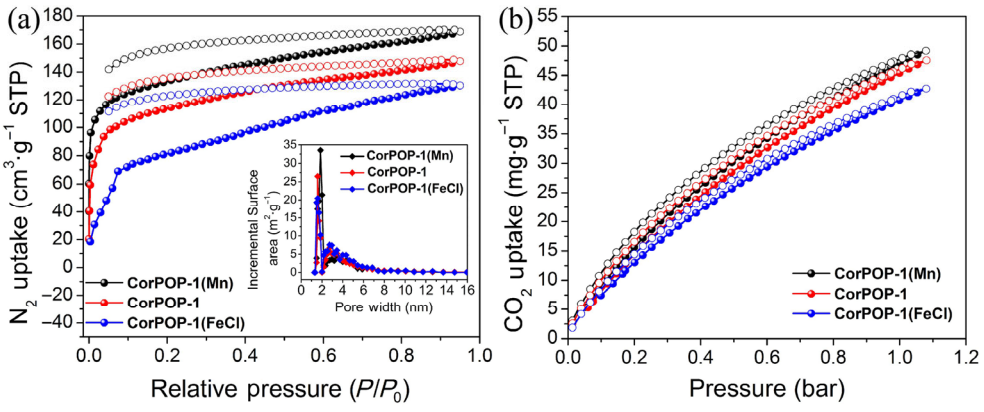

Figure 3 (a) N_2 sorption isotherms and pore size distributions (inset) for CorPOPs at 77 K. (b) CO_2 sorption isotherms for CorPOPs at 298 K.

3.3 Evaluation of catalytic performance

Meallocorroles represent a burgeoning class of metal-complexes widely employed in catalysis [16–22], and the heterogenization of them would overcome the drawbacks that homogeneous systems encounter and achieve a high density of isolated catalytically active centers. Nevertheless, the incorporation of metallocorroles as the molecular building units into porous solid supports by the bottom-up approach applied for heterogeneous organocatalysis has barely been reported [32] albeit highly promising. Considering that CO_2 is an abundant, nontoxic, and inexpensive C1 feedstock, the efficient transformation of CO_2 into value-added chemicals is very attractive both industrially and academically [40–42]. The catalytic CO_2 cycloaddition with epoxides [43–45] has been consumingly investigated because of its highly atom-economic effect and the wide applications of the produced cyclic carbonates in pharmaceutical [46, 47] and fine chemical [48–50] industries. Recent advances have been made in demonstrating the good catalytic activity of metallocorroles for this reaction under atmospheric pressure and at relatively low temperature even room temperature [21], due to their ability to stabilize coordinated metal ions in higher oxidation states, whereas for metalloporphyrins, high pressure (> 6 bar) and temperature (> 100 °C) system conditions are generally needed in the reaction processes [51–53]. Therefore, with the combination of large surface areas, permanent porosity, exceptional stability, and the capability to capture CO_2, and strong metallocorrole Lewis acid active sites in CorPOPs, we decided to investigate their catalytic performance in the cycloaddition of epoxides into CO_2 to form cyclic carbonates.

As shown in Table 1 and Table S3 in the ESM, the system involving the **CorPOP-1(Mn)** and cocatalyst TBAB shows superior catalytic activity in the conversion of 1,2-butylene oxide to the corresponding cyclic carbonate under mild reaction conditions, far outperforming those of all other catalytic systems. The MnPFBC/**CorPOP-1(Mn)** without the addition of the TBAB exhibited no catalytic capability (Table 1, entries 1 and 4). In the absence of MnPFBC/**CorPOP-1(Mn)**, the TBAB alone afforded only 5% yield in the CO_2 cycloaddition reaction (Table 1, entry 2). However, when combing the monomer MnPFBC or **CorPOP-1(Mn)** with TBAB, MnPFBC catalyzed the reaction with 72% yield in the homogeneous system (Table 1, entry 3), whereas a remarkably higher yield of 98% can be achieved when prompted by the heterogeneous catalyst **CorPOP-1(Mn)** (Table 1, entry 5). The porous structure of the CO_2-capturing heterogeneous nanocatalyst facilitates the enrichment of CO_2 near metallcorrole catalytic centers located in the polymeric skeleton, which, together with the existence of isolated and high-density active sites likely accounts

Table 1 Cycloaddition of CO_2 with 1,2-butylene oxide catalyzed over various reaction systems[a]

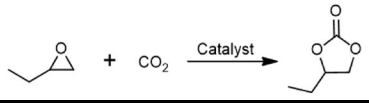

Entry	Catalyst (mol.%)	TBAB (mol.%)	Yield (%)[f]
1[b]	MnPFBC (0.1%)	—	n.r.
2	Blank	4%	5
3[b]	MnPFBC (0.1%)	4%	72
4[c]	**CorPOP-1(Mn)** (0.1%)	—	n.r.
5[c]	**CorPOP-1(Mn)** (0.1%)	4%	98
6[d]	**CorPOP-1** (0.1%)	4%	6
7[e]	**CorPOP-1(FeCl)** (0.1%)	4%	45

[a]Reaction conditions: 1,2-butylene oxide (940 mg, 13 mmol), CO_2 (1 bar), TBAB (168 mg, 0.52 mmol), 40 °C, and 12 h. [b]10.7 mg of MnPFBC (0.013 mmol). [c]10.8 mg of **CorPOP-1(Mn)** (0.013 mmol MnCor active sites). [d]10.1 mg of **CorPOP-1** (0.013 mmol Cor units). [e]11.2 mg of **CorPOP-1(FeCl)** (0.013 mmol FeClCor active sites). [f]The percentage yields were evaluated from the ^{1}H NMR spectra by integration of epoxide versus cyclic carbonate peaks. n.r. = no reaction.

for the enhanced catalytic reactivity of **CorPOP-1(Mn)** compared with MnPFBC. Furthermore, we implemented their kinetic catalytic experiments (Fig. 4(a)), and the results can intuitively illustrate the advantages of heterogenizing MnPFBC catalyst for CO_2 chemical fixation. As a control experiment, metal-free **CorPOP-1** in the presence of TBAB showed no obvious catalytic activity (Table 1, entry 6), which confirmed the vital role of metallcorroles in activating the reactant. Further study was conducted with **CorPOP-1(FeCl)** as the active species toward catalyzing this reaction, resulting in a much lower yield (45%) than **CorPOP-1(Mn)** (Table 1, entry 7). We reasoned that the prominent discrepancy in the catalytic efficiency should be mainly attributed to both the altered Lewis acidity influenced by coordination metals and the presence of the counter chloride anion in the metallocorrole monomer of **CorPOP-1(FeCl)** blocking the accessibility to the open Lewis Fe site [54, 55].

The recyclability was tested by using the recycled **CorPOP-1(Mn)** catalyst, which is deemed to be an essential characteristic when one catalyst is considered for potential use in industrial applications. To minimize the effect of the small amount of catalyst in a reaction on the final cycling yield, experiments were performed employing a large excess of 1,2-butylene oxide (65 mmol) and **CorPOP-1(Mn)** (0.065 mmol, 54 mg) with the maintained reaction conditions (40 °C and 1 bar of CO_2). Recycling results indicated that no significant decrease of the catalytic activity of **CorPOP-1(Mn)** was observed

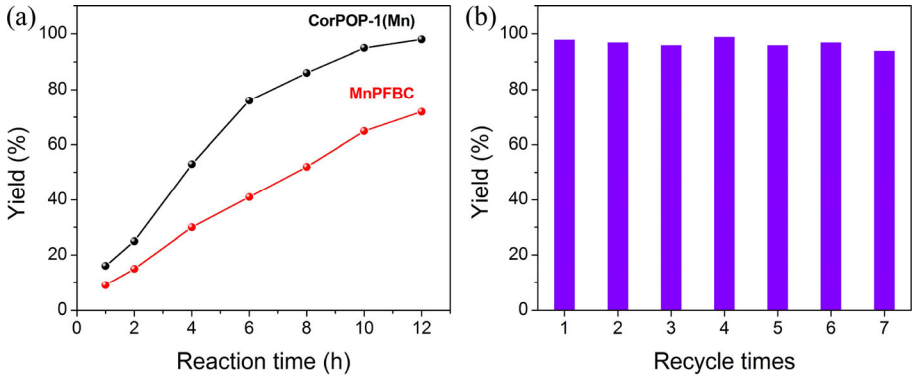

Figure 4 (a) The product (1,2-butylene carbonate) yield depending on reaction time under atmospheric pressure at 40 °C catalyzed by **CorPOP-1(Mn)** and MnPFBC. (b) Recyclability of **CorPOP-1(Mn)** toward the cycloaddition of CO_2 to 1,2-butylene oxide.

even after seven successive cycles (Fig. 4(b)), highlighting its heterogeneous nature. Moreover, the recycled catalyst displayed similar N_2 sorption isotherms with the comparable BET surface area and porosity to the pristine sample (Fig. S14 in the ESM). The SEM images revealed that the morphology of **CorPOP-1(Mn)** after catalysis remained almost unchanged (Fig. S15 in the ESM). ICP-OES showed that its Mn content (5.9 wt.%) was only slightly lower than that of the original catalyst. Additionally, the catalyst recovery efficiency for **CorPOP-1(Mn)** after the first reaction was 98% and retained as high as 85% even after seven cycles. The above results thus highlight **CorPOP-1(Mn)** as an excellent reusable and stable heterogeneous catalyst.

On the basis of the previously reported mechanisms of the cycloaddition of CO_2 with epoxides [21], a tentative **CorPOP-1(Mn)**-based catalytic mechanism for this coupling reaction is presented in Fig. S16 in the ESM. The catalytic center (Mn-corrole) was clipped from **CorPOP-1(Mn)**. We performed DFT calculations covering the energy profiles of the intermediates and their predicted geometries in the stationary phase, to support the proposed mechanism (Fig. S17 in the ESM). The catalytic cycle begins with the activation of epoxides by the Lewis Mn-corrole sites to form the intermediate **A**, and then, the bromide anion promotes the ring-opening of epoxides to produce metal/heteroatom alkoxide intermediate **B**. Subsequently, a Mn carbonate intermediate **C** is formed through the insertion of CO_2 into the Mn–O bond of the opened ring. Finally, the reaction process is completed by an intramolecular ring-closure step to yield the products and the regenerated catalyst.

Encouraged by the outstanding catalytic activity of **CorPOP-1(Mn)**, we expanded the scope of epoxide substrates. All of the tested substrates were converted into their corresponding cyclic carbonate products in high yields under mild reaction conditions (Table 2). It is notable that the reaction involved in the propylene oxide/epichlorohydrin can smoothly proceeded, wherein the comprehensive catalytic effects are comparable with those reported POPs also having accessible active metal sites and some other typical catalysts (Tables S4 and S5 in the ESM). Additionally, CO_2 cycloaddition with 3-butenyloxirane or glycidyl phenyl ether gave the much lower turnover frequency (TOF) values relative to those of the other epoxides-containing reactions in this work (Table S6 in the ESM). These results reveal that the large-size epoxides are restricted by the pore sizes of polymeric catalyst that would influence the transport of the substrates and products through the pores, thus leading to decreased TOF values. Overall, the excellent catalytic efficiency and good substrate compatibility make **CorPOP-1(Mn)** a promising heterogeneous catalyst for CO_2 fixation to afford valuable products.

Table 2 **CorPOP-1(Mn)** catalyzed cycloaddition reactions of various epoxides with atmospheric CO_2 to form cyclic carbonates[a]

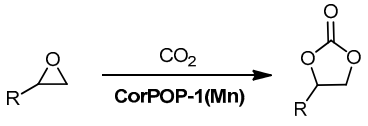

Entry	Epoxides	Products	T (°C)	t (h)	Yield (%)[b]
1		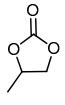	25	16	96
2		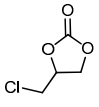	40	12	97
3	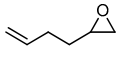	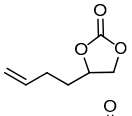	40	24	93
4	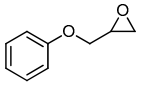	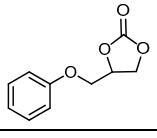	80	40	99

[a]Reaction conditions: epoxide (13 mmol), CO_2 (1 bar), TBAB (0.52 mmol), and **CorPOP-1(Mn)** (10.8 mg, containing 0.013 mmol MnCor active sites). [b]The yields were determined by ^{1}H NMR.

4 Conclusion

To conclude, we have reported the design and synthesis of corrole-based POPs featuring permanent porosity and prominent stability as well as the investigation of them as heterogeneous catalysts for CO_2 fixation. Specifically, the immobilization of catalytically active species MnPFBC as the building unit in the polymeric skeleton integrated with the structural merits of POP supports endows **CorPOP-1(Mn)** with excellent catalytic performance in the context of CO_2 cycloaddition to form cyclic carbonates under mild reaction conditions, far outperforming the homogeneous counterpart, with good substrate compatibility and excellent recyclability. This work represents a successful attempt to explore novel nanoporous solid materials while combining the abilities to capture and convert CO_2 efficiently. We expect that our study will not only spur interest in the construction of heterogeneous catalysts toward carbon fixation, but also promote future development of corrole- functionalized porous materials in a broader range of applications.

Acknowledgements

This work was supported by the National Natural Science foundation of China (NSFC) (22078241) and China Scholarship

Council (CSC) (No. 201706250095). Partial support from the Robert A. Welch Foundation (B-0027) is also acknowledged (SM).

Electronic Supplementary Material: Supplementary material (further experimental details, characterizations, ^{1}H NMR spectrum, single crystal data, UV–Vis absorption spectra, TGA curves, PXRD patterns, FTIR spectra, solid-state ^{13}C CP/MAS NMR spectra, SEM images, catalytic study, DFT calculations, etc.) is available in the online version of this article at https://doi.org/10.1007/s12274-021-3617-3.

References

[1] Urbani, M.; Grätzel, M.; Nazeeruddin, M. K.; Torres, T. Meso-substituted porphyrins for dye-sensitized solar cells. *Chem. Rev.* **2014**, *114*, 12330–12396.

[2] Shimizu, D.; Osuka, A. Porphyrinoids as a platform of stable radicals. *Chem. Sci.* **2018**, *9*, 1408–1423.

[3] Singh, S.; Aggarwal, A.; Bhupathiraju, N. V. S. D. K.; Arianna, G.; Tiwari, K.; Drain, C. M. Glycosylated porphyrins, phthalocyanines, and other porphyrinoids for diagnostics and therapeutics. *Chem. Rev.* **2015**, *115*, 10261–10306.

[4] Baglia, R. A.; Zaragoza, J. P. T.; Goldberg, D. P. Biomimetic reactivity of oxygen-derived manganese and iron porphyrinoid complexes. *Chem. Rev.* **2017**, *117*, 13320–13352.

[5] Almeida-Marrero, V.; van de Winckel, E.; Anaya-Plaza, E.; Torres, T.; de la Escosura, A. Porphyrinoid biohybrid materials as an emerging toolbox for biomedical light management. *Chem. Soc. Rev.* **2018**, *47*, 7369–7400.

[6] Koszarna, B.; Gryko, D. T. Efficient synthesis of meso-substituted corroles in a H_2O-MeOH mixture. *J. Org. Chem.* **2006**, *71*, 3707–3717.

[7] Thomas, K. E.; Alemayehu, A. B.; Conradie, J.; Beavers, C. M.; Ghosh, A. The structural chemistry of metallocorroles: Combined X-ray crystallography and quantum chemistry studies afford unique insights. *Acc. Chem. Res.* **2012**, *45*, 1203–1214.

[8] Ghosh, A. Electronic structure of corrole derivatives: Insights from molecular structures, spectroscopy, electrochemistry, and quantum chemical calculations. *Chem. Rev.* **2017**, *117*, 3798–3881.

[9] Mahammed, A.; Gross, Z. Corroles as triplet photosensitizers. *Coord. Chem. Rev.* **2019**, *379*, 121–132.

[10] Aviv, I.; Gross, Z. Corrole-based applications. *Chem. Commun.* **2007**, 1987–1999.

[11] Haber, A.; Gross, Z. Catalytic antioxidant therapy by metallodrugs: Lessons from metallocorroles. *Chem. Commun.* **2015**, *51*, 5812–5827.

[12] Zhang, W.; Lai, W. Z.; Cao, R. Energy-related small molecule activation reactions: Oxygen reduction and hydrogen and oxygen evolution reactions catalyzed by porphyrin- and corrole-based systems. *Chem. Rev.* **2017**, *117*, 3717–3797.

[13] Teo, R. D.; Hwang, J. Y.; Termini, J.; Gross, Z.; Gray, H. B. Fighting cancer with corroles. *Chem. Rev.* **2017**, *117*, 2711–2729.

[14] Aviv-Harel, I.; Gross, Z. Coordination chemistry of corroles with focus on main group elements. *Coord. Chem. Rev.* **2011**, *255*, 717–736.

[15] Nardis, S.; Mandoj, F.; Stefanelli, M.; Paolesse, R. Metal complexes of corrole. *Coord. Chem. Rev.* **2019**, *388*, 360–405.

[16] Lei, H. T.; Li, X. L.; Meng, J.; Zheng, H. Q.; Zhang, W.; Cao, R. Structure effects of metal corroles on energy-related small molecule activation reactions. *ACS Catal.* **2019**, *9*, 4320–4344.

[17] Mahammed, A.; Gray, H. B.; Meier-Callahan, A. E.; Gross, Z. Aerobic oxidations catalyzed by chromium corroles. *J. Am. Chem. Soc.* **2003**, *125*, 1162–1163.

[18] Haber, A.; Mahammed, A.; Fuhrman, B.; Volkova, N.; Coleman, R.; Hayek, T.; Aviram, M.; Gross, Z. Amphiphilic/bipolar metallocorroles that catalyze the decomposition of reactive oxygen and nitrogen species, rescue lipoproteins from oxidative damage, and attenuate atherosclerosis in mice. *Angew. Chem.* **2008**, *120*, 8014–8018.

[19] Mahammed, A.; Gross, Z. Highly efficient catalase activity of metallocorroles. *Chem. Commun.* **2010**, *46*, 7040–7042.

[20] Kuwano, T.; Kurahashi, T.; Matsubara, S. Iron corrole-catalyzed [4 + 2] cycloaddition of dienes and aldehydes. *Chem. Lett.* **2013**, *42*, 1241–1243.

[21] Tiffner, M.; Gonglach, S.; Haas, M.; Schöfberger, W.; Waser, M. CO_2 fixation with epoxides under mild conditions with a cooperative metal corrole/quaternary ammonium salt catalyst system. *Chem. Asian J.* **2017**, *12*, 1048–1051.

[22] Guo, M.; Lee, Y. M.; Gupta, R.; Seo, M. S.; Ohta, T.; Wang, H. H.; Liu, H. Y.; Dhuri, S. N.; Sarangi, R.; Fukuzumi, S. et al. Dioxygen activation and O-O bond formation reactions by manganese corroles. *J. Am. Chem. Soc.* **2017**, *139*, 15858–15867.

[23] Yang, L. J.; Shui, J. L.; Du, L.; Shao, Y. Y.; Liu, J.; Dai, L. M.; Hu, Z. Carbon-based metal-free ORR electrocatalysts for fuel cells: Past, present, and future. *Adv. Mater.* **2019**, *31*, 1804799.

[24] Bavykina, A.; Kolobov, N.; Khan, I. S.; Bau, J. A.; Ramirez, A.; Gascon, J. Metal−organic frameworks in heterogeneous catalysis: Recent progress, new trends, and future perspectives. *Chem. Rev.* **2020**, *120*, 8468–8535.

[25] Liu, J. G.; Wang, N.; Ma, L. L. Recent advances in covalent organic frameworks for catalysis. *Chem. Asian J.* **2020**, *15*, 338–351.

[26] Sun, Q.; Dai, Z. F.; Meng, X. J.; Xiao, F. S. Porous polymer catalysts with hierarchical structures. *Chem. Soc. Rev.* **2015**, *44*, 6018–6034.

[27] Banerjee, S.; Anayah, R. I.; Gerke, C. S.; Thoi, V. S. From molecules to porous materials: Integrating discrete electrocatalytic active sites into extended frameworks. *ACS Cent. Sci.* **2020**, *6*, 1671–1684

[28] Zhang, Y. G.; Ying, J. Y. Main-chain organic frameworks with advanced catalytic functionalities. *ACS Catal.* **2015**, *5*, 2681–2691.

[29] Slater, A. G.; Cooper, A. I. Function-led design of new porous materials. *Science* **2015**, *348*, aaa8075.

[30] Lee, J. S. M.; Cooper, A. I. Advances in conjugated microporous polymers. *Chem. Rev.* **2020**, *120*, 2171–2214.

[31] Tian, Y. Y.; Zhu, G. S. Porous aromatic frameworks (PAFs). *Chem. Rev.* **2020**, *120*, 8934−8986.

[32] Zhao, Y. M.; Qi, S. B.; Niu, Z.; Peng, Y. L.; Shan, C.; Verma, G.; Wojtas, L.; Zhang, Z. J.; Zhang, B.; Feng, Y. Q. et al. Robust corrole-based metal−organic frameworks with rare 9-connected Zr/Hf-oxo clusters. *J. Am. Chem. Soc.* **2019**, *141*, 14443−14450.

[33] Friedman, A.; Landau, L.; Gonen, S.; Gross, Z.; Elbaz, L. Efficient bio-inspired oxygen reduction electrocatalysis with electropolymerized cobalt corroles. *ACS Catal.* **2018**, *8*, 5024–5031.

[34] Khan, R.; Idris, M.; Tuncel, D. Synthesis and investigation of singlet oxygen production efficiency of photosensitizers based on *meso*-phenyl-2,5-thienylene linked porphyrin oligomers and polymers. *Org. Biomol. Chem.* **2015**, *13*, 10496–10504.

[35] Tang, A. L.; Li, L. J.; Lu, Z. H.; Huang, J. H.; Jia, H.; Zhan, C. L.; Tan, Z. A.; Li, Y. F.; Yao, J. N. Significant improvement of photovoltaic performance by embedding thiophene in solution-processed star-shaped TPA-DPP backbone. *J. Mater. Chem. A* **2013**, *1*, 5747–5757.

[36] Gershman, Z.; Goldberg, I.; Gross, Z. DNA Binding and catalytic properties of positively charged corroles. *Angew. Chem., Int. Ed.* **2007**, *46*, 4320–4324.

[37] Liu, H. Y.; Chen, L.; Yam, F.; Zhan, H. Y.; Ying, X.; Wang, X. L.; Jiang, H. F.; Chang, C. K. Reductive demetalation of manganese corroles: The substituent effect. *Chin. Chem. Lett.* **2008**, *19*, 1000–1003.

[38] Zhao, Y. M.; Dai, W. H.; Peng, Y. L.; Niu, Z.; Sun, Q.; Shan, C.; Yang, H.; Verma, G.; Wojtas, L.; Yuan, D. Q. et al. A corrole-based covalent organic framework featuring desymmetrized topology. *Angew. Chem., Int. Ed.* **2020**, *59*, 4354–4359.

[39] Ju, P. Y.; Wu, S. J.; Su, Q.; Li, X. D.; Liu, Z. Q.; Li, G. H.; Wu, Q. L. Salen–porphyrin-based conjugated microporous polymer supported Pd nanoparticles: Highly efficient heterogeneous catalysts for aqueous C–C coupling reactions. *J. Mater. Chem. A* **2019**, *7*, 2660–2666.

[40] Artz, J.; Müller, T. E.; Thenert, K.; Kleinekorte, J.; Meys, R.; Sternberg, A.; Bardow, A.; Leitner, W. Sustainable conversion of carbon dioxide: An integrated review of catalysis and life cycle assessment. *Chem. Rev.* **2018**, *118*, 434−504.

[41] Hou, S. L.; Dong, J.; Jiang, X. L.; Jiao, Z. H.; Zhao, B. A noble-metal-free metal–organic framework (MOF) catalyst for the highly efficient conversion of CO_2 with propargylic alcohols. *Angew. Chem., Int. Ed.* **2019**, *58*, 577−581.

[42] Cao, C. S.; Xia, S. M.; Song, Z. J.; Xu, H.; Shi, Y.; He, L. N.; Cheng, P.; Zhao, B. Highly efficient conversion of propargylic amines and CO_2 catalyzed by noble-metal-free [Zn_{116}] nanocages. *Angew. Chem., Int. Ed.* **2020**, *132*, 8664−8671.

[43] Kamphuis, A. J.; Picchioni, F.; Pescarmona, P. P. CO_2-fixation into cyclic and polymeric carbonates: Principles and applications. *Green Chem*. **2019**, *21*, 406–448.
[44] Shaikh, R. R.; Pornpraprom, S.; D'Elia, V. Catalytic strategies for the cycloaddition of pure, diluted, and waste CO_2 to epoxides under ambient conditions. *ACS Catal*. **2018**, *8*, 419−450.
[45] Dong, J.; Cui, P.; Shi, P. F.; Cheng, P.; Zhao, B. Ultrastrong alkali-resisting lanthanide-zeolites assembled by [Ln_{60}] nanocages. *J. Am. Chem. Soc*. **2015**, *137*, 15988−15991.
[46] Tortajada, A.; Juliá-Hernández, F.; Börjesson, M.; Moragas, T.; Martin, R. Transition-metal-catalyzed carboxylation reactions with carbon dioxide. *Angew. Chem., Int. Ed*. **2018**, *57*, 15948–15982.
[47] Nielsen, D. U.; Hu, X. M.; Daasbjerg, K.; Skrydstrup, T. Chemically and electrochemically catalysed conversion of CO_2 to CO with follow-up utilization to value-added chemicals. *Nat. Catal*. **2018**, *1*, 244–254.
[48] Liu, Q.; Wu, L. P.; Jackstell, R.; Beller, M. Using carbon dioxide as a building block in organic synthesis. *Nat. Commun*. **2015**, *6*, 5933.
[49] Guo, W. S.; Gómez, J. E.; Cristòfol, À.; Xie, J. N.; Kleij, A. W. Catalytic transformations of functionalized cyclic organic carbonates. *Angew. Chem., Int. Ed*. **2018**, *57*, 13735–13747.
[50] Song, L.; Jiang, Y. X.; Zhang, Z.; Gui, Y. Y.; Zhou, X. Y.; Yu, D. G. CO_2 = CO + [O]: Recent advances in carbonylation of C–H bonds with CO_2. *Chem. Commun*. **2020**, *56*, 8355–8367.
[51] Ema, T.; Miyazaki, Y.; Shimonishi, J.; Maeda, C.; Hasegawa, J. Y. Bifunctional porphyrin catalysts for the synthesis of cyclic carbonates from epoxides and CO_2: Structural optimization and mechanistic study. *J. Am. Chem. Soc*. **2014**, *136*, 15270–15279.
[52] Jin, L. L.; Jing, H. W.; Chang, T.; Bu, X. L.; Wang, L.; Liu, Z. L. Metal porphyrin/phenyltrimethylammonium tribromide: Highly efficient catalysts for coupling reaction of CO_2 and epoxides. *J. Mol. Catal. A: Chem*. **2007**, *261*, 262–266.
[53] Bai, D. S.; Duan, S. H.; Hai, L.; Jing, H. W. Carbon dioxide fixation by cycloaddition with epoxides, catalyzed by biomimetic metalloporphyrins. *ChemCatChem* **2012**, *4*, 1752–1758.
[54] Johnson, J. A.; Petersen, B. M.; Kormos, A.; Echeverría, E.; Chen, Y. S.; Zhang, J. A new approach to non-coordinating anions: Lewis acid enhancement of porphyrin metal centers in a zwitterionic metal–organic framework. *J. Am. Chem. Soc*. **2016**, *138*, 10293–10298.
[55] Alkordi, M. H.; Weseliński, Ł. J.; D'Elia, V.; Barman, S.; Cadiau, A.; Hedhili, M. N.; Cairns, A. J.; AbdulHalim, R. G.; Basset, J. M.; Eddaoudi, M. CO_2 conversion: The potential of porous-organic polymers (POPs) for catalytic CO_2–epoxide insertion. *J. Mater. Chem. A* **2016**, *4*, 7453– 7460.